How does radiofrequency ablation efficacy depend on the stiffness of the cardiac tissue? Insights from a computational model

Argyrios Petras[1,*], Massimiliano Leoni[1,2], Jose M. Guerra[3], Johan Jansson[1,2], and Luca Gerardo-Giorda[1]

[1]BCAM - Basque Center for Applied Mathematics, Bilbao, Spain
[2]Department of Computational Science and Technology, KTH Royal Institute of Technology, Stockholm, Sweden
[3]Department of Cardiology, Hospital de la Santa Creu i Sant Pau, Barcelona, Spain
[*]Alameda de Mazarredo 14, 48009 Bilbao, Bizkaia, Spain, apetras@bcamath.org

February 27th, 2019

Abstract

Objective. Radiofrequency catheter ablation (RFCA) is an effective treatment for the elimination of cardiac arrhythmias, however it is not exempt from complications that can risk the patients' life. The efficacy of the RFCA depends on several factors and uncertainties during the treatment process. In this paper, we explore the effect of the cardiac tissue stiffness in RFCA.

Methods. We use our previously developed RFCA computational model that accounts for the tissue elasticity. The tissue stiffness is described by the Young's modulus of elasticity.

Results. Our numerical simulations provide insights on the efficacy of the RFCA, by measuring the lesion dimensions over a wide range of values of the modulus of elasticity that appear during the cardiac cycle and for different cardiac conditions, using a fixed ablation protocol, commonly used in clinical practice.

Conclusion. The stiffness of the cardiac wall affects the power dissipated in the tissue and, as a consequence, has a marked effect on the dimensions of the generated lesion. The heart wall elasticity changes due the cardiac cycle can affect the resulting lesion and can lead to potentially dangerous complications. Pathological conditions can stiffen the cardiac wall, thus reducing the size of the resulting lesion and potentially leading to insufficient treatment.

Significance. A relation of the lesion size dimensions for different tissue stiffness and contact force is presented and correlated to different pathological conditions of the heart, showing the direct relation of the tissue stiffness with the efficacy of the RFCA treatment.

Keywords: radiofrequency ablation, computational model, open-irrigated catheter, tissue elasticity, Young's modulus.

1 Introduction

Radiofrequency ablation (RFA) using open-irrigated catheters is a common treatment for different types of cardiac arrhythmias. RFA is typically a safe procedure, yet life-threatening complications can occur, including coagulum formation when the blood proteins denature at 80 °C and steam formation when the tissue reaches 100 °C, resulting in audible steam pops [17]. Several in-silico sOur numerical simulations provide insights on the efficacy of the RFCA over a wide range of values of the modulus of elasticity that appear during the cardiac cycle and for different cardiac conditions, using a fixed ablation protocol.tudies have been developed to model the biophysics of the RFA and to provide insights for the prevention of these adverse conditions [2, 4, 8, 10, 11, 26]. Most of these models overlook the deformation of the tissue in contact with the catheter. A recent model was introduced that includes the mechanical properties of the tissue [20], and has been validated against in-vitro experimental results. A comparison of the elastic deformation of the tissue against the sharp insertion of the catheter at an undeformed tissue showed the importance of the inclusion of the mechanical properties in RFA models [20, 21].

One of the parameters that affect the power delivery and the tissue deformation is the Young's modulus of elasticity, which describes the stiffness of the tissue. The accurate identification of the Young's modulus of elasticity for soft tissues is a challenging task. Several techniques are used to this end, including lamb wave dispersion ultrasound vibrometry [27], real-time shear wave elastography [6] and supersonic shear imaging [5]. A large variation between the Young's modulus of different soft tissues appears in the literature [28]. In particular, the identification of the elasticity of the cardiac muscle is extremely difficult due to its structure and the cardiac cycle (systole and diastole). There are studies that consider in-vitro measurements [22, 25], where there is no effect of the heartbeat. Other studies that include ex-vivo and in-vivo situations show clearly a dependence of the Young's modulus on the phase of the cardiac cycle [5, 16, 19, 27].

The cardiac muscle has a complex structure and consists of fibers whose 120° transmural shift in orientation leads to an anisotropic Young's modulus [15]. Furthermore, the stiffness of the myocardium can be affected by pathological conditions. Specifically, different heart diseases, such as mitral stenosis, aortic insufficiency, and cardiac hypertrophy, tend to make the cardiac wall stiffer [9].

In this paper, we explore the effect of the stiffness of the cardiac tissue in the RFA process. We consider the model in [20] and a homogenous, isotropic cardiac tissue. Different aspects of the RFA are investigated, including the tissue deformation due to the contact with the catheter, the power dissipation in the tissue and the size of the resulting lesion.

2 Model summary

2.1 Geometry

A full three-dimensional computational geometry is considered that consists of the blood chamber, the cardiac tissue, a board that models effects external to the system, the electrode and the thermistor, as shown in Figure 1 left. A six-hole open-irrigated electrode is considered with a hemispherical tip, following the design of state-of-the-art catheters typically used for RFA. Figure 1 right shows the computational composition of the electrode in our model.

The cardiac tissue undergoes a mechanical deformation due to the contact with the catheter,

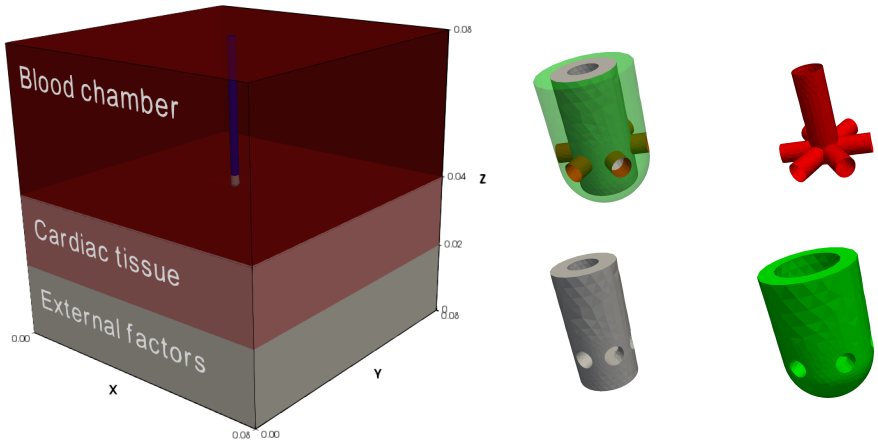

Figure 1: Left: The full computational geometry. Right: The computational tip of the catheter (top left), the saline tubes (top right), the thermistor (bottom left) and the electrode (bottom right).

which is described using an axisymmetric Boussinesq solution for a spherical profile for a given contact force F [24]. In particular, the relation of the force, the contact radius a of the electrode and the tissue and the maximum indentation depth $\omega_{\max}$ is given by:

$$F = \frac{G}{1-\nu}\left((a^2+R^2)\log\left(\frac{R+a}{R-a}\right) - 2aR\right),$$

where

$$\omega_{\max} = \frac{a}{2}\log\left(\frac{R+a}{R-a}\right),$$

R being the radius of the electrode, G the shear modulus and ν the Poisson's ratio. The shear modulus is related to the Young's modulus of elasticity E as:

$$G = \frac{E}{2(1+\nu)}.$$

The vertical deformation of the tissue is described as:

$$\omega(r) = \begin{cases} \omega_{\max} - (R - \sqrt{R^2 - r^2}), & r \le a, \\ \dfrac{a^2}{\pi}\displaystyle\int_0^1 \frac{2\omega_{\max} - at\log\left(\frac{R+at}{R-at}\right)}{r^2 - a^2t^2}\,dt, & r > a, \end{cases}$$

and is directly imposed on the tissue geometry.

2.2 Mathematical model

The incompressible Navier-Stokes equations describe the blood flow and interaction of the blood and the irrigated saline from the electrode holes. Specifically:

$$\begin{aligned} \frac{\partial \mathbf{u}}{\partial t} + \mathbf{u} \cdot \nabla \mathbf{u} - \operatorname{div} \sigma(\mathbf{u}, p) &= \mathbf{0} && \text{in } \Omega_{blood} \times (0, T), \\ \operatorname{div} \mathbf{u} &= 0 && \text{in } \Omega_{blood} \times (0, T), \end{aligned}$$

where $\mathbf{u}$ is the flow velocity, $\sigma(\cdot, \cdot)$ is the stress tensor, p is the pressure scaled by the density and Ω_{blood} is the blood subdomain. A constant blood inflow is considered at the plane $X = 0$ of the blood subdomain with the corresponding outflow conditions at $X = 0.08$ (see Figure 1). A radial inflow towards the blood is considered from the blood-saline pipes interface. No slip conditions are imposed on all surfaces, including the internal blood-tissue interface.

The temperature changes are modelled using a modified version of Penne's bioheat equation in the whole computational domain:

$$\rho c(T) \left(\frac{\partial T}{\partial t} + \mathbf{u} \cdot \nabla T \right) - \operatorname{div}(k(T) \nabla T) = \sigma(T) |\nabla \Phi|^2,$$

where T is the temperature, ρ is the density, c is the specific heat, k is the thermal conductivity, $\sigma(\cdot)$ is the electrical conductivity and Φ is the electrical potential. Thermal insulation boundary conditions are applied on the catheter walls and the saline pipes, while a constant temperature of 22 °C is considered on the blood-pipes interface. Body temperature of 37 °C is applied on all the remaining boundaries.

The electrical potential is governed by a quasi-static equation augmented with a constraint for constant power ablation in the whole computational domain Ω:

$$\begin{cases} \operatorname{div}(\sigma(T) \nabla \Phi) = 0, \\ \\ \displaystyle\int_\Omega \sigma(T) |\nabla \Phi|^2 \, dx = P, \end{cases}$$

where P is the total power dissipated in our system. A potential V_0 is considered on the catheter-electrode interface, which is calculated via optimization techniques to satisfy the power constraint equation [20]. Zero potential at the bottom of the computational domain models the dispersive electrode, while insulation boundary conditions are applied to all remaining boundaries.

A more detailed analysis of the mathematical model can be found in [20].

2.3 Parameters

A number of parameters appear in the mathematical model that are drawn from the literature [11, 12, 28] and summarized in SI units in Table 1. A porcine cardiac tissue is considered in this work. The electrical conductivity of the board underneath the tissue σ_b is tuned to match the initial resistance of the system and power delivered to the tissue P_{tissue}, which can be calculated using the formula:

$$P_{tissue} = \frac{A_{tissue} \sigma_{tissue}}{A_{blood} \sigma_{blood} + A_{tissue} \sigma_{tissue}} P_0 =: \alpha P_0, \tag{1}$$

where P_0 is the total power set by the ablation protocol, (A_{blood}, σ_{blood}) and (A_{tissue}, σ_{tissue}) are the contact area of the electrode with the blood and the tissue respectively, along with the corresponding electrical conductivities. More details can be found in [20].

Table 1: The summary of the parameters used in the model in SI units.

	Blood	Tissue	Electrode	Thermistor	Board
ρ ($\mathrm{kg\,m^{-3}}$)	1050	1076	21500	32	1076
c ($\mathrm{J\,kg^{-1}\,K^{-1}}$)	3617	c_0	132	835	3017
k ($\mathrm{W\,m^{-1}\,K^{-1}}$)	0.52	k_0	71	0.038	0.518
σ ($\mathrm{S\,m^{-1}}$)	0.748	σ_0	4.6×10^{6}	10^{-5}	σ_b
μ ($\mathrm{kg\,m^{-1}\,s^{-1}}$)	2.52×10^{-6}	-	-	-	-
ν (-)	-	0.499	-	-	-

A linear relation with the temperature is considered for the thermal and electrical properties of the porcine tissue, as derived from [3, 7]

$$c(T) = c_0(1 - 0.0042(T - 37)),$$

$$k(T) = k_0(1 - 0.0005(T - 37)),$$

$$\sigma(T) = \sigma_0(1 + 0.015(T - 37)),$$

where $c_0 = 3017\,\mathrm{J\,kg^{-1}\,K^{-1}}$, $k_0 = 0.518\,\mathrm{W\,m^{-1}\,K^{-1}}$ and $\sigma_0 = 0.54\,\mathrm{S\,m^{-1}}$ are the values at body temperature.

3 Results

In our numerical experiments, a constant power ablation protocol of 20 W is considered for a total of 30 s. Such protocol is commonly performed in clinical RFA. The saline irrigation rate is set to 17 ml/ min and the blood flow to $0.5\,\mathrm{m\,s^{-1}}$. The open source programs FEniCS-HPC [13, 14, 18], Salome [23] and Paraview [1] are used for the numerical simulations, as detailed in [20].

We first explore theObjective. Radiofrequency catheter ablation (RFCA) is an effective treatment for the elimination of cardiac arrhythmias, however it is not exempt from complications that can risk the patients' life. The efficacy of the RFCA depends on several factors and uncertainties during the treatment process. In this paper, we explore the effect of the cardiac tissue stiffness in RFCA.

Methods. We use our previously developed RFCA computational model that accounts for the tissue elasticity. The tissue stiffness is described by the Young's modulus of elasticity.

Results. Our numerical simulations provide insights on the efficacy of the RFCA, by measuring the lesion dimensions over a wide range of values of the modulus of elasticity that appear during the cardiac cycle and for different cardiac conditions, using a fixed ablation protocol.

Conclusion. The stiffness of the cardiac wall affects the power dissipated in the tissue and, as a consequence, has a marked effect on the dimensions of the generated lesion. The heart wall elasticity changes due the cardiac cycle can affect the resulting lesion and can lead to potential dangerous complications. Pathological conditions can stiffen the cardiac wall, thus reducing the size of the resulting lesion and potentially leading to insufficient treatment.

Significance. A relation of the lesion size dimensions for different tissue stiffness and contact force is presented and correlated to different pathological conditions of the heart, showing the direct relation of the tissue stiffness with the efficacy of the RFA treatment. effect of the tissue elasticity on the computational geometry of our RFA model. The Young's modulus describes the stiffness of the cardiac wall and affects the indentation depth of the catheter within the tissue. Specifically, Figure 2 shows the deformation of the tissue interface for a constant force of 10 g and different values of the Young's modulus of elasticity that typically appear during the systole (top row of Figure 2) and the diastole (bottom row of Figure 2) of the cardiac cycle [5, 16, 19, 27]. Note that for small values of the Young's modulus, a larger part of the electrode is in contact with the tissue. Indeed, Figure 3 left shows the contact percentage of the outer surface area of the electrode with the tissue. Due to discretization limitations, a contact of the electrode with the tissue is considered when the tissue surface is very close to the electrode, which corresponds to an approximation error that exists due to the finite element construction of our computational geometry. A minimum element aspect ratio of 6 is considered in this work.

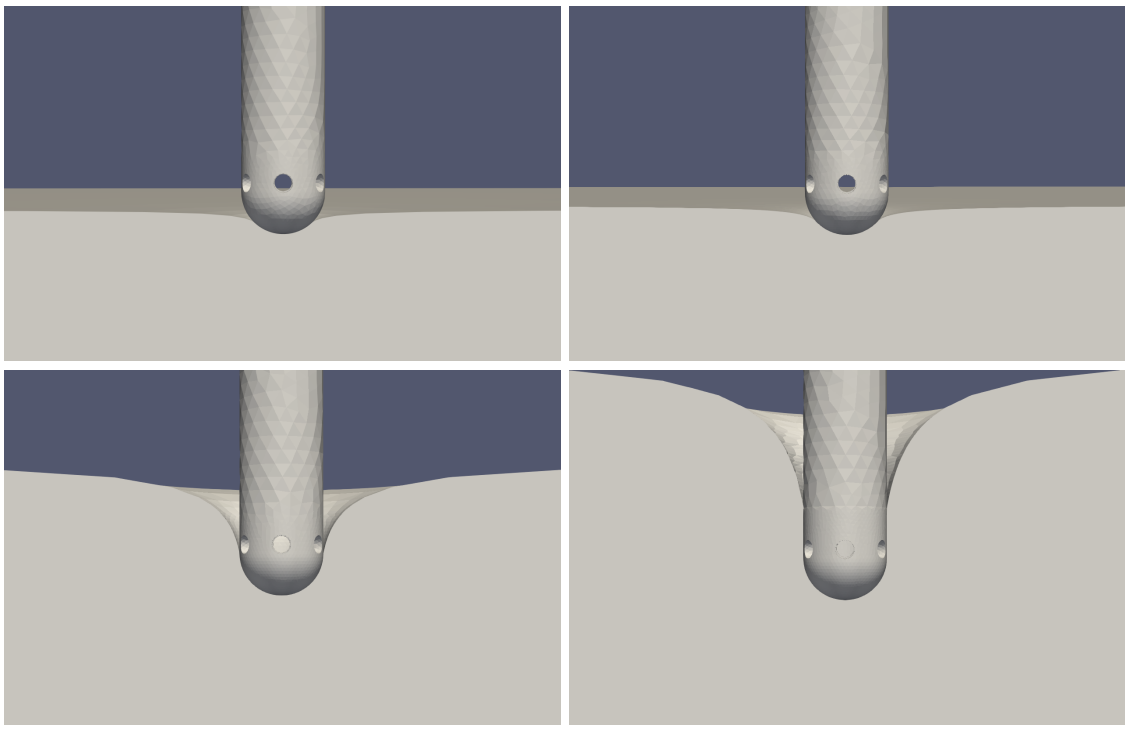

Figure 2: The indentation of the tissue by applying 10 g force using a Young's modulus of 100 kPa, 75 kPa, 10 kPa and 5 kPa (top left to bottom right).

The increase in the electrode-tissue contact percentage results in a change in the amount of power dissipated in the tissue [20, 29]: the larger the electrode-tissue contact, the larger the power delivered to the tissue. Indeed, Figure 3 right shows the power percentage dissipated in the tissue for the parameters described in a previous section. There are minor changes in the power

delivery for large values of the Young's modulus (around 100 kPa), which appear typically in the systole phase. However, the power percentage change becomes more significant for diastole Young's modulus values near 10 kPa.

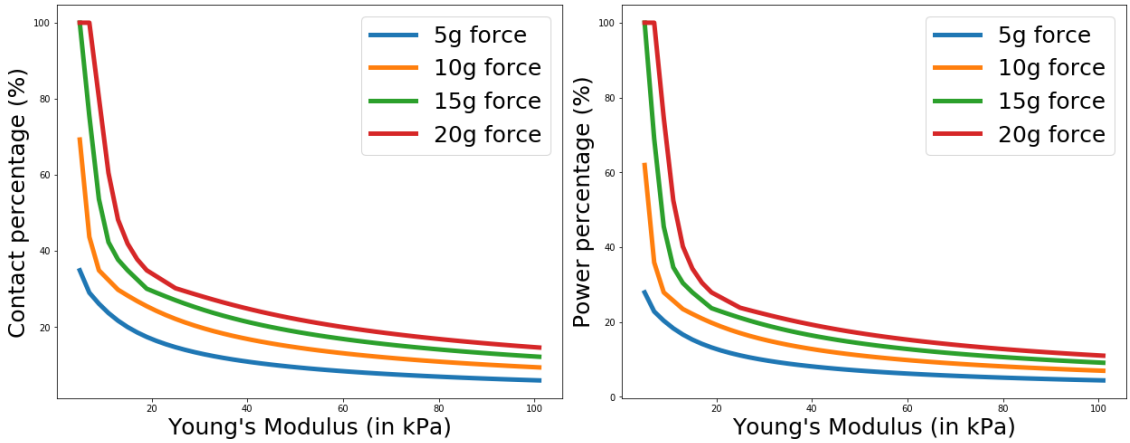

Figure 3: The electrode-tissue contact percentage (left) and the power percentage delivered to the tissue (right) for different values of Young's modulus and force.

The effect of the Young's modulus of elasticity becomes evident during the ablation process. Table 2 shows the depth (D), the width (W), the depth at the maximum width (DW), the surface area of the lesion on the blood-tissue interface (S) and the volume (V) of the ablation lesion, as described in [20]. The quantity α is the power percentage dissipated in the tissue at the beginning of the ablation, defined in (1). As an example, in the 100 kPa case the power dissipated in the tissue initially is 1.398 W, while at 10 kPa the corresponding value is 5.578 W. Observe that the lesion size is much smaller in the systole cases, while the lesion becomes much larger for Young's modulus' values that correspond to the diastole phase. However, both cases with low elastic modulus 10 kPa and 5 kPa lead to complications. In particular, a steam pop occurrence at 28.2 s appears in the 10 kPa case, while in the 5 kPa case the formation of a coagulum is present, with the blood temperature reaching 80 °C after 0.8 s. For stiffer tissues, the temperature remains well below 100 °C in the tissue and 80 °C in the blood. Figure 4 shows a cross section of the lesions that appear in Table 2.

A relation of the Young's modulus with the depth and the width of the lesion for different applied-force ablation protocols is explored in Figure 5, where the filled markers denote a successful 30 s ablation without complications and the empty markers a steam pop occurrence. As the cardiac tissue becomes more elastic, the depth and the width of the lesion are becoming larger up to a point where too much power is dissipated in the tissue and its temperature reaches 100 °C before the completion of the 30 s. A consistent increase of the depth and the width of the lesion also appears with the increase of the contact force. However, extreme overheating of the tissue occurs in the case of a very elastic cardiac tissue with 10 kPa modulus of elasticity, for contact forces larger than 5 g.

There are some limitations in the present study. All the deformations that appear in this work are considered purely elastic. An isotropic homogenous tissue is considered, even though

Table 2: The summary of the lesion size dimensions for different Young's modulus profiles at the final time of the simulation or at the pop occurrence.

Quantity	Systole		Diastole	
	100 kPa	75 kPa	10 kPa	5 kPa
α (%)	6.99	8.46	27.89	61.94
$\omega_{\max}$ (mm)	0.67	0.81	3.82	6.91
D (mm)	2.02	2.58	4.54	0.87
W (mm)	4.04	4.88	10.88	4.59
DW (mm)	0.43	0.80	-0.45	-3.53
S (mm^2)	0	0	3.71	11.07
V (mm^3)	20.1	38.3	448.7	37.7
$T_{\max}$ tissue (°C)	56.6	61.2	100.0	76.4
$T_{\max}$ blood (°C)	46.9	45.2	60.5	80.0
t_{pop} (s)	-	-	28.2	0.8

the cardiac wall microheterogeneities might have an effect on the tissue deformation. Moreover, the cardiac tissue consists of fibers of changing orientation along the transverse direction [15]. Our computational model is built from an *in-vitro* experimental setup and thus the cardiac tissue is fixed. In *in-vivo* situations, the cardiac wall movement affects both the Young's modulus of elasticity and possibly the contact force. The inclusion of the movement of the cardiac wall in the RFA model is part of our ongoing work.

4 Conclusion

A range of different values for the cardiac wall stiffness are considered that are reported during the systole and diastole phases of the cardiac cycle, which impact the tissue deformation, the amount of the electrode in direct contact with the tissue and the power dissipated in the tissue. For large values of the Young's modulus, small changes occur in the indentation depth and the power delivered to the tissue. Much larger changes appear for more elastic tissues, where the amount of power dramatically increases.

The stiffness of the cardiac wall affects the power dissipated in the tissue and has a marked effect on the dimensions of the generated lesion. Our simulations show that small lesions appear for stiff tissues, as they receive a smaller amount of power. On the contrary, large lesions and potential complications occur during the ablation with low Young's modulus, where the temperature reaches 100 °C before the completion of 30 s. Especially in the case of 5 kPa, there is a high risk of thrombus formation very early in the procedure, since the blood temperature reaches 80 °C after the completion of only 0.8 s of ablation.

To study the efficacy of the RFA process, the width and the depth of the lesion were assessed for different tissue stiffnesses, under a constant ablation protocol. Our results show that the lesion dimensions become significantly smaller for stiffer tissues. This can have a serious impact when performing RFA treatment on patients with any one of a number of heart conditions, such as cardiac hypertrophy, aortic stenosis or mitral stenosis. As an example, the cardiac muscle of a patient with aortic stenosis is about 10 times stiffer than that of a patient with mitral stenosis [9].

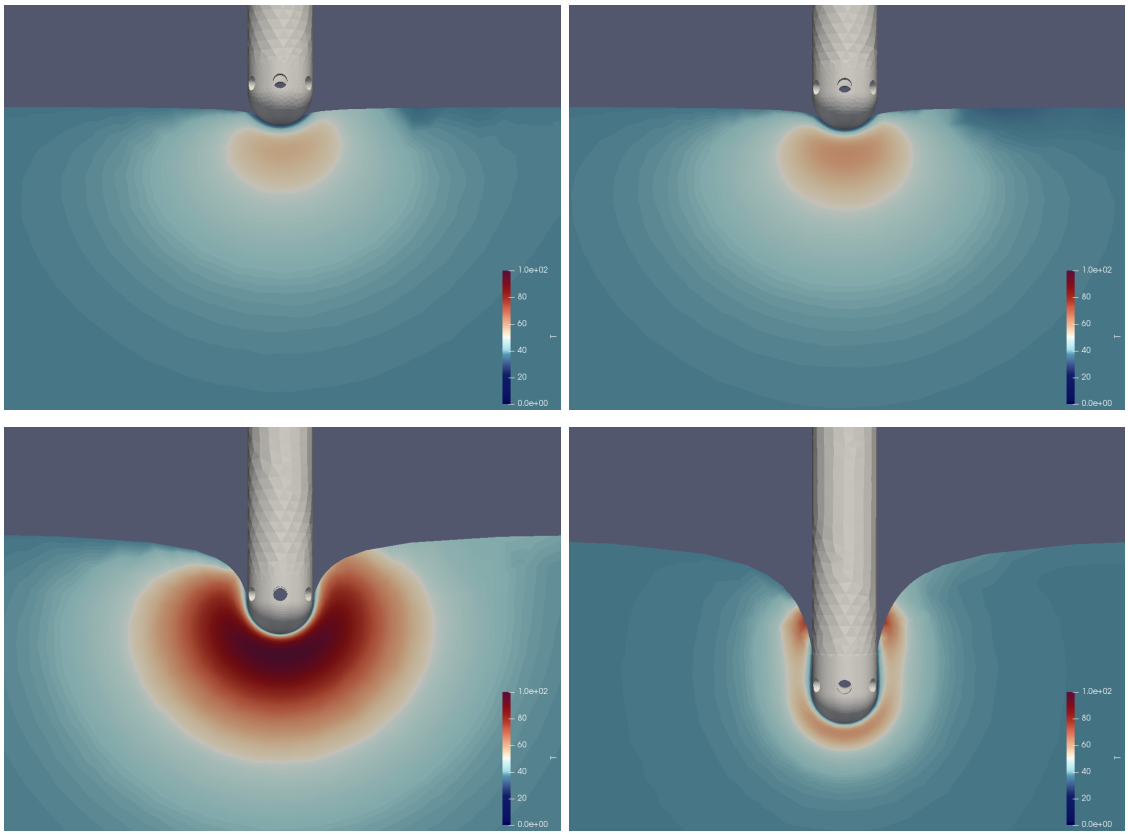

Figure 4: A visualization of the lesions for the systole (top) and diastole (bottom) values for the Young's modulus. From top left to bottom right the Young's modulus considered is 100 kPa, 75 kPa, 10 kPa and 5 kPa.

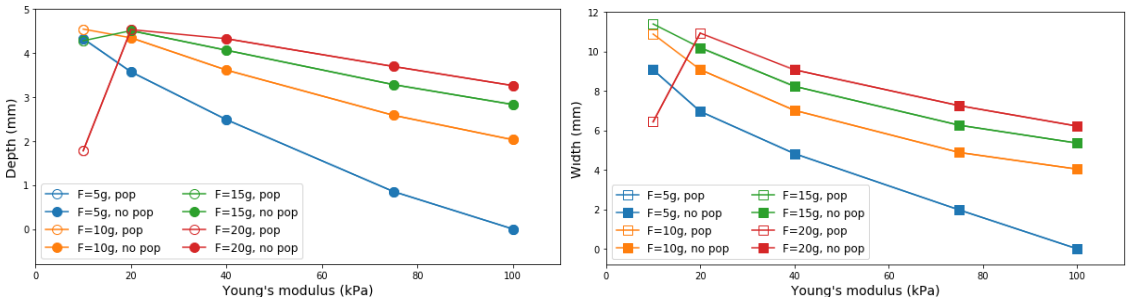

Figure 5: The depth and width of the lesion for different values of the Young's modulus of elasticity at the final time of the ablation or at the pop occurrence.

Thus, for an effective treatment, different ablation protocols should be considered based on the cardiac wall stiffness.

Acknowledgment

This research was supported by the Basque Government through the BERC 2014-2017 and BERC 2018-2021 program and by Spanish Ministry of Economy and Competitiveness MINECO through BCAM Severo Ochoa excellence accreditations SEV-2013-0323 and SEV-2017-0718, and through projects MTM2015-69992-R and MTM2016-76016-R. ML acknowledges the "LaCaixa 2016" PhD Grant.

References

[1] Utkarsh Ayachit. *The paraview guide: a parallel visualization application*. Kitware, Inc., 2015.

[2] Enrique J Berjano. Theoretical modeling for radiofrequency ablation: state-of-the-art and challenges for the future. *Biomedical engineering online*, 5(1):24, 2006.

[3] NC Bhavaraju and JW Valvano. Thermophysical properties of swine myocardium. *International journal of thermophysics*, 20(2):665–676, 1999.

[4] Hong Cao, Michael A Speidel, Jang-Zern Tsai, Michael S Van Lysel, Vicken R Vorperian, and John G Webster. Fem analysis of predicting electrode-myocardium contact from rf cardiac catheter ablation system impedance. *IEEE Transactions on Biomedical Engineering*, 49(6):520–526, 2002.

[5] Mathieu Couade, Mathieu Pernot, Mickael Tanter, Emmanuel Messas, Alain Bel, Maguette Ba, Albert-Alain Hagège, and Mathias Fink. Quantitative imaging of myocardium elasticity using supersonic shear imaging. In *Ultrasonics Symposium (IUS), 2009 IEEE International*, pages 151–154. IEEE, 2009.

[6] YB Deng, QY Tang, J Sun, and W Zhou. Quantification of shear modulus in in vitro porcine myocardium using real-time shear wave elastography. *Ultrasound in Medicine and Biology*, 39(5):S28, 2013.

[7] Francis A Duck. *Physical properties of tissues: a comprehensive reference book*. Academic press, 2013.

[8] Neal Gallagher, Elise C Fear, Israel A Byrd, and Edward J Vigmond. Contact geometry affects lesion formation in radio-frequency cardiac catheter ablation. *PloS one*, 8(9):e73242, 2013.

[9] Dhanjoo N Ghista, West H Vayo, and Harold Sandler. Elastic modulus of the human intact left ventricle-determination and physiological interpretation. *Medical and biological engineering*, 13(2):151–161, 1975.

[10] A González-Suárez and Enrique Berjano. Comparative analysis of different methods of modeling the thermal effect of circulating blood flow during rf cardiac ablation. *IEEE Transactions on Biomedical Engineering*, 63(2):250–259, 2016.

[11] Ana González-Suárez, Enrique Berjano, Jose M Guerra, and Luca Gerardo-Giorda. Computational modeling of open-irrigated electrodes for radiofrequency cardiac ablation including blood motion-saline flow interaction. *PloS one*, 11(3):e0150356, 2016.

[12] P.A. Hasgall, E. Neufeld, M.C. Gosselin, A. Klingenböck, and N. Kuster. Itis database for thermal and electromagnetic parameters of biological tissues. *Version 3.0*, 2015.

[13] Johan Hoffman, Johan Jansson, and Niclas Jansson. Fenics-hpc: Automated predictive high-performance finite element computing with applications in aerodynamics. *Proceedings of the 11th International Conference on Parallel Processing and Applied Mathematics, PPAM 2015. Lecture Notes in Computer Science*, 2015.

[14] Johan Hoffman, Johan Jansson, Niclas Jansson, Rodrigo Vilela De Abreu, and Claes Johnson. Computability and adaptivity in cfd. *Encyclopedia of Computational Mechanics Second Edition*, pages 1–22, 2017.

[15] Brent K Hoffmeister, Scott M Handley, Samuel A Wickline, and James G Miller. Ultrasonic determination of the anisotropy of youngs modulus of fixed tendon and fixed myocardium. *The Journal of the Acoustical Society of America*, 100(6):3933–3940, 1996.

[16] Peter J Hollender, Patrick D Wolf, Robi Goswami, and Gregg E Trahey. Intracardiac echocardiography measurement of dynamic myocardial stiffness with shear wave velocimetry. *Ultrasound in medicine & biology*, 38(7):1271–1283, 2012.

[17] Shoei K Stephen Huang and Mark A Wood. *Catheter Ablation of Cardiac Arrhythmias E-book*. Elsevier Health Sciences, 2014.

[18] Anders Logg, Kent-Andre Mardal, Garth Wells, and et. al. Automated solution of differential equations by the finite element method. *Lecture Notes in Computational Science and Engineering*, 84:1–736, 2012.

[19] Ivan Z Nenadic, Matthew W Urban, Cristina Pislaru, Daniel Escobar, Luiz Vasconcelos, and James F Greenleaf. In vivo open-and closed-chest measurements of left-ventricular myocardial viscoelasticity using lamb wave dispersion ultrasound vibrometry (lduv): a feasibility study. *Biomedical Physics & Engineering Express*, 4(4):047001, 2018.

[20] Argyrios Petras, Massimiliano Leoni, Jose M Guerra, Johan Jansson, and Luca Gerardo-Giorda. A computational model of open-irrigated radiofrequency catheter ablation accounting for mechanical properties of the cardiac tissue. *International Journal for Numerical Methods in Biomedical Engineering (submitted)*, 2018.

[21] Argyrios Petras, Massimiliano Leoni, Guerra Ramos JM, Johan Jansson, and Luca Gerardo-Giorda. Effect of tissue elasticity in cardiac radiofrequency catheter ablation models. *Computing in Cardiology Conference (CinC)*, 2018.

[22] Sherif Ramadan, Narinder Paul, and Hani E Naguib. Standardized static and dynamic evaluation of myocardial tissue properties. *Biomedical Materials*, 12(2):025013, 2017.

[23] Andre Ribes and Christian Caremoli. Salome platform component model for numerical simulation. In *Computer Software and Applications Conference, 2007. COMPSAC 2007. 31st Annual International*, volume 2, pages 553–564. IEEE, 2007.

[24] Ian N Sneddon. The relation between load and penetration in the axisymmetric boussinesq problem for a punch of arbitrary profile. *International journal of engineering science*, 3(1):47–57, 1965.

[25] Qiaoying Tang, Youbin Deng, Kun Liu, Jun Zhang, Yuan Huang, and Jie Sun. Quantification of shear modulus in in vitro porcine myocardium using real-time shear wave elastography. *Chinese Journal of Ultrasonography*, 21(8):708–710, 2012.

[26] Zhen Tian, Qun Nan, Xiaohui Nie, Tong Dong, and Ruirui Wang. The comparison of lesion outline and temperature field determined by different ways in atrial radiofrequency ablation. *Biomedical engineering online*, 15(2):124, 2016.

[27] Matthew W Urban, Cristina Pislaru, Ivan Z Nenadic, Randall R Kinnick, and James F Greenleaf. Measurement of viscoelastic properties of in vivo swine myocardium using lamb wave dispersion ultrasound vibrometry (lduv). *IEEE transactions on medical imaging*, 32(2):247–261, 2013.

[28] Peter NT Wells and Hai-Dong Liang. Medical ultrasound: imaging of soft tissue strain and elasticity. *Journal of the Royal Society Interface*, 8(64):1521–1549, 2011.

[29] Fred HM Wittkampf and Hiroshi Nakagawa. Rf catheter ablation: Lessons on lesions. *Pacing and Clinical Electrophysiology*, 29(11):1285–1297, 2006.